eprints@whiterose.ac.uk
https://eprints.whiterose.ac.uk/

Robotic Autonomy for Magnetic Endoscope Biopsy

James W. Martin[1][*], Lavinia Barducci[1], Bruno Scaglioni[1], Joseph C. Norton[1], Conchubhair Winters[2], Venkataraman Subramanian[2], Alberto Arezzo[3], Keith L. Obstein[4], and Pietro Valdastri[1]

Abstract—Magnetically actuated endoscopes are currently transitioning in to clinical use for procedures such as colonoscopy, presenting numerous benefits over their conventional counterparts. Intelligent and easy-to-use control strategies are an essential part of their clinical effectiveness due to the un-intuitive nature of magnetic field interaction. However, work on developing intelligent control for these devices has mainly been focused on general purpose endoscope navigation. In this work, we investigate the use of autonomous robotic control for magnetic colonoscope intervention via biopsy, another major component of clinical viability. We have developed control strategies with varying levels of robotic autonomy, including semi-autonomous routines for identifying and performing targeted biopsy, as well as random quadrant biopsy. We present and compare the performance of these approaches to magnetic endoscope biopsy against the use of a standard flexible endoscope on bench-top using a colonoscopy training simulator and silicone colon model. The semi-autonomous routines for targeted and random quadrant biopsy were shown to reduce user workload with comparable times to using a standard flexible endoscope.

Index Terms—Medical robotics, Endoscopes, Autonomous systems, Robot control, Medical device.

I. INTRODUCTION

Colonsocopy is the standard investigative modality for addressing the high prevalence and incidence of gastrointestinal diseases [1]. The procedure allows for visual inspection of the colon for signs of disease, tissue biopsies to be taken for pathological examination, as well as the resection of abnormal tissue growths such as polyps which, when removed in early stages, can preclude the onset of Colorectal Cancer (CRC), the third most common malignancy worldwide, and second leading cause of cancer related deaths [2]. Unfortunately, shortcomings in the aging design of the Flexible Endoscope

[1]STORM Lab UK, University of Leeds, Leeds, UK. *Corresponding email: j.martin3@leeds.ac.uk
[2]Leeds Teaching Hospitals NHS Trust, St James's University Hospital, Leeds, UK.
[3]Department of Surgical Sciences, University of Torino, Turin, Italy.
[4]STORM Lab USA, Vanderbilt University, Nashville, TN, USA. 5 Vanderbilt University Medical Center, Nashville, TN, USA.

(FE) used for this procedure [3], [4] have contributed to difficulties in reducing CRC incidence.

In response, magnetically actuated endoscopes have been developed to address these issues and improve access to high quality colonoscopy. They show potential in reducing pain (removing the need for sedation), lowering cost, and can exhibit a short learning curve [5] due to simplified controls and robotic autonomy. They allow for a single use approach, maintain the ability to provide therapeutic intervention, with the added possibility of enhancing diagnostic capabilities [6]. A significant contributor to the clinical translation of these devices is the involvement of intelligent magnetic control methodologies; the inclusion of which is necessary to improve ease-of-use and exemplify a high-standard colonoscopy provider [7].
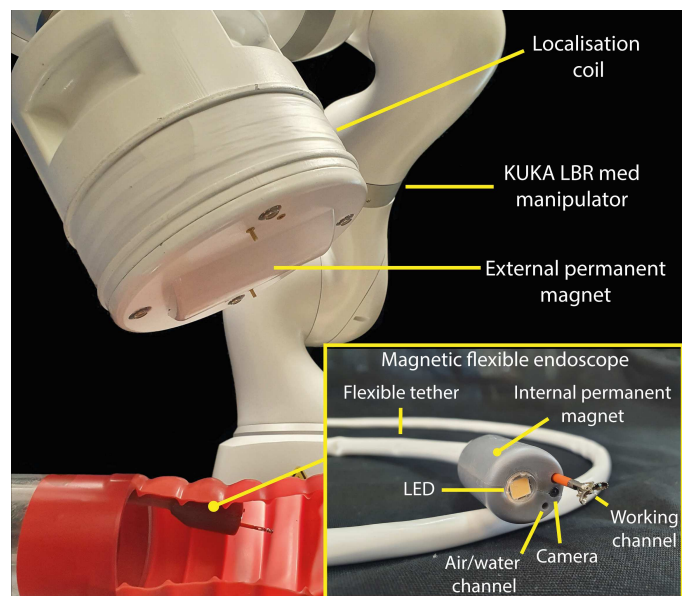
Fig. 1. Overview of the Magnetic Flexible Endoscope (MFE) system. The magnetic endoscope (bottom right) contains a camera, LED, and an insufflation, irrigation, and working channel. A KUKA LBR Med robotic arm actuates the MFE via manipulating an external permanent magnet mounted to its end effector.

Magnetic endoscopes are controlled by varying extracorporeal magnetic fields, generated by electromagnetic coils, or by permanent magnets commonly mounted on robotic manipulators [8], as shown in Fig. 1. The involvement of assistive control is necessary due to these fields being non-linearly related to the motion of the magnetic endoscope. Having the user directly control the state of the actuating field to guide the endoscope without assistance is un-intuitive, slow, and ineffective [7], [9]. Development in this area of

intelligent control for magnetic colonoscopy has mainly been concerned with general endoscope navigation [7], [10], [11], or has addressed other procedural aspects of colonoscopy such as retroflexion [12]. The use of biopsy, another major procedural component, is currently devoid of intelligent magnetic control and has mainly been shown to demonstrate design function-ality concepts in wired [13], [14], [15], and wireless devices [16], with work on autonomy demonstrated in a non-magnetic crawler robot in a large colon simulator system [17].

Biopsy during colonoscopy can be categorised in to tar-geted, or random biopsy [18]. For wired devices this involves passing biopsy forceps down a tool channel from the proximal end of the scope until protruding from the distal tip. When performing targeted biopsy, the protruding forceps are aligned to an area of suspicious tissue where the user exerts the forceps upon the target site, closing and rapidly withdrawing the forceps to take a sample. In contrast, random biopsies do not target tissue specifically, but are taken in multiple colon regions at specific intervals, from numerous quadrants relating to 4 evenly spaced points around the circumference of the colon. The most involved example of performing random quadrant biopsy is with surveillance of pancolitis, where biopsies of the four quadrants are recommended throughout the colon at 10 cm intervals, with a minimum total of 33 biopsies [18]. Typically, an endoscopist will reach the end of the colon (the ceacum) as fast as possible, and then perform tasks such as biopsy when withdrawing the endoscope from the colon.

An operators ability to effectively perform multi-scenario targeted or random quadrant biopsy with a magnetic endo-scope is a necessary component of their clinical viability for colonoscopy. The ability to specifically orientate the scope, as well as target a small lesion (less than 3-4 mm in size) can be challenging due to the endoscopes configuration within the colon, and the position of the lesion in relation to where the instrument (biopsy forceps) emerges from the colonoscope. The ability to maintain stability and position within this convoluted environment to efficiently take biopsies takes great skill and cognitive ability. This opens the way for improving the process through automation. Therefore, in this work we contribute with the development and investigation of assistive robotic autonomy for targeted and random quadrant biopsy for magnetically actuated endoscopes, being applicable to platforms with real-time endoscope pose detection and other devices pertaining to robotic colonoscopy. Moreover, this work is transferable to similar endoscopic robotic systems where biopsy in unstructured environments is required, such as bronchoscopy and gastroscopy. We investigate the perfor-mance of magnetic endoscope biopsy with varying levels of assistive-robotic autonomy, compared against the use of a standard flexible endoscope. With this, we demonstrate how the inclusion of robotic autonomy contributes to the clinical performance of these devices.

To demonstrate this work, we make use of the Magnetic Flexible Endoscope (MFE) platform shown in Fig. 1, and further described in Section. II-A. We have developed a semi-autonomous routine for targeted biopsy which comprises of the system automatically locating and tracking a tissue target

with the endoscope on-board camera. The depth to the target is then extracted using a stereo-vision approach, which is used to predict the tip location of the biopsy forceps, projected out from the endoscope tool-channel at that same depth. Following this, the system autonomously aligns the magnetic endoscope using a permanent magnet mounted to the end-effector of a robotic manipulator. This autonomously aligns the tissue target to the predicted tip location of the forceps, allowing the user to simply acquire the tissue target, manually pushing, closing and retracting the forcep jaws. Secondly, we have implemented an autonomous routine to subsequently align the magnetic endoscope tool channel to each colon quadrant for random biopsy. We evaluated these methods on bench-top, and included repetitions as a comparison in each scenario where the operator is directly responsible for controlling the orientation of the MFE camera via a joystick, referred to as "Closed-loop tele-operation" [7]. Additionally for comparison, each scenario included repetitions where the operator was to perform random and targeted biopsy using a standard flexible endoscope.

II. MATERIALS AND METHODS

In this section we describe the MFE platform used in this work, and the theoretical formulations of the closed-loop robotic and magnetic system, used to impart torque as a desired change in orientation of the MFE camera frame. Following this, we described the semi-autonomous routines for targeted and random quadrant biopsy using the MFE.

A. Magnetic flexible endoscope system

The MFE system shown in Fig. 1 comprises a small Intracorporeal Permanent Magnet (IPM) embedded in 3-D printed shell tip that encapsulates a camera (465x580 pixels) and LED. This shell tip is then attached to a highly flexible tether containing cabling, and an insufflation and irrigation channel. A working channel is also present to pass down flexible tools such as biopsy forceps. Actuation is achieved by imparting magnetic forces and torques upon the MFE to change its position and orientation by adjusting the pose of an Extracorporeal Permanent Magnet (EPM) mounted to the end effector of a robotic manipulator (KUKA LBR Med R820). A flexible circuit surrounds the IPM with a strategically placed array of Hall effect sensors and an Inertial Measurement Unit (IMU) used for endoscope localisation. The resulting Hall-effect and IMU sensory information of the MFE, given as an effect of its current pose in the presence the EPM magnetic field, combined with an additional non-actuating field produced from an electromagnetic coil that surrounds the EPM allows for the pose of the MFE to be estimated in real time (100Hz), in 6-DOF, with a positional and rotational accuracy of 5mm ($\pm$1mm) and 6° ($\pm$0.8°), respectively [19]. This positional information is vital for intelligent closed-loop, and autonomous control strategies.

B. Endoscope control

The robotic end-effector/EPM is controlled in Cartesian space by means of an incremental algorithm. At every time-step, the position variation δp_e and heading increment $\widehat{\delta m_e}$,

with respect to the previous step, are computed and sent to the robot low-level controller. The magnetic interaction between the EPM and IPM is modelled using the magnetic-dipole model [20], and builds upon previous work [7]. Locally, the rotational interaction can be linearised and described as a change in torque exerted on the IPM by a displacement of the EPM:

$$
\begin{aligned}
\delta \boldsymbol{\tau_i} &= \begin{bmatrix} \frac{\partial \boldsymbol{\tau_m}}{\partial \boldsymbol{p_e}} & \frac{\partial \boldsymbol{\tau_m}}{\partial \widehat{\boldsymbol{m_e}}} \end{bmatrix} \begin{bmatrix} \delta \boldsymbol{p_e} \\ \delta \widehat{\boldsymbol{m_e}} \end{bmatrix} \\
&= \boldsymbol{J_{m,\tau}} \begin{bmatrix} \delta \boldsymbol{p_e} \\ \delta \widehat{\boldsymbol{m_e}} \end{bmatrix}
\end{aligned}
\tag{1}
$$

where $\delta \boldsymbol{\tau_i}$ are variations of torques applied to the endoscope, $\boldsymbol{\tau_m}$ is the nonlinear expression of torques in the dipole model, a function of $\boldsymbol{p_e}$, $\widehat{\boldsymbol{m_e}}$ and of the position and orientation of the IPM, and $\boldsymbol{J_{m,\tau}}$ is the linearised local relation for given EPM and IPM poses $(\boldsymbol{p_e}, \boldsymbol{p_i}, \widehat{\boldsymbol{m_e}}, \widehat{\boldsymbol{m_i}})$.

Rotational displacements of the EPM end effector are computed as follows:

$$
\begin{aligned}
\delta \widehat{\boldsymbol{m_e}} &= \boldsymbol{J_{m,\tau}^{\dagger}} \boldsymbol{R_G^I} \gamma \boldsymbol{K_\tau} \begin{bmatrix} \delta \boldsymbol{\theta_y} \\ \delta \boldsymbol{\theta_z} \end{bmatrix} \\
&+ (1-\gamma)[k_{pf} P_{xy}(\widehat{\boldsymbol{m_e}} - \widehat{\boldsymbol{m_i}}) \\
&+ k_{if} \int_0^t P_{xy}(\widehat{\boldsymbol{m_e}} - \widehat{\boldsymbol{m_i}})dt]
\end{aligned}
\tag{2}
$$

Eq. 2 describes the heading control law. The heading change requested by the higher-level control on the Y-Z plane in the MFE camera frame, $\delta \boldsymbol{\theta_y}$ and $\delta \boldsymbol{\theta_z}$, are weighted by means of the diagonal matrix $\boldsymbol{K_\tau}$ and rotated in the global reference frame by the rotation matrix $\boldsymbol{R_G^I}$. Finally, the Moore-Pensore pseudoinverse of the local magnetic coupling $\boldsymbol{J_{m,\tau}}$ is applied to compute the rotation. The second part of the equation is associated to a linear motion request of the EPM, used during manual withdrawal of the MFE from the colon to align the magnets and keep them within close proximity to each other. This functionality, referred to as "Magnetic follower", is further described in Section II-C1.

C. Targeted biopsy

This routine comprises several elements that are combined to autonomously detect and align a tissue target to the tool channel of the MFE. Once aligned, the user is prompted to exert and close the biopsy forceps on the target, which are then withdrawn to acquire a sample. The semi-autonomous sequence is shown in Fig. 2, with the following components further described in their corresponding subsections, where:

- II-C1 *Magnetic Follower*: Will cause the robot/EPM to follow the IPM autonomously as the user withdraws the MFE by pulling back on the endoscope tether.
- II-C2 *Target detection*: Automatically detects and tracks a suspicious tissue target in real-time using the MFE camera.
- II-C3 *Stereo target position estimation*: Computes the distance from the MFE to the tissue target, using concepts of a stereo vision system.

- II-C4 *Instrument alignment*: Uses this distance information to impart torque upon the IPM, via the EPM, such that a tool channel projection of the MFE is aligned to the tissue target, and a biopsy can be taken.
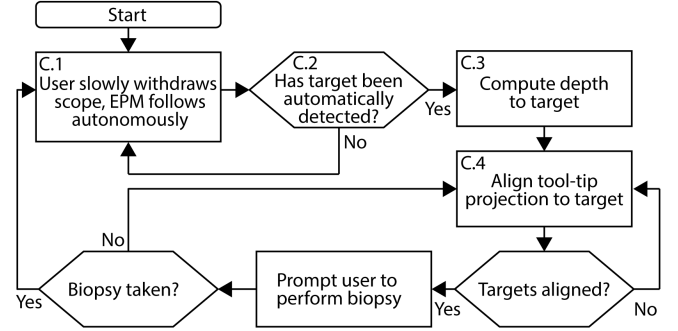

Fig. 2. Flowchart of MFE semi-autonomous targeted biopsy routine.

1) Magnetic follower: When no other action is commanded, the system will enter a "magnet following" state whereby the robot will maintain an EPM position directly above the IPM. When the user withdraws the MFE by slowly pulling on the endoscope tether, the EPM will follow above and align to the heading of the IPM autonomously. This keeps the system in an "always ready" state whereby the effectiveness of subsequent torque imparted on the MFE to change its orientation can be immediately optimised.

In the second part of Eq. 2, a binary value, $\gamma \in [0, 1]$, is associated to a linear motion request of the EPM with a Proportional-integral (PI) controller with proportional gain K_{pf} and integral gain K_{if}. This is activated if there is no input to the orientation controller ($\gamma = 0$), i.e. during manual withdrawal of the MFE from the colon. The magnets are aligned with the difference in heading between the two magnets projected on the global horizontal plane (XY). The linear displacement of the EPM is described as:

$$
\delta \boldsymbol{p_e} = K_{pr} \begin{bmatrix} P_{e,x} - P_{i,x} \\ P_{e,y} - P_{i,y} \end{bmatrix} + K_{ir} \int_0^t \begin{bmatrix} P_{e,x} - P_{i,x} \\ P_{e,y} - P_{i,y} \end{bmatrix} dt
\tag{3}
$$

and uses a PI controller, with proportional gain K_{pr} and integral gain K_{ir}.

2) Target detection: To automatically detect and track suspicious tissue in real-time, we trained an object detection system (YOLOv3) [21] to recognise and track lesions, trained with a data set of 300 annotated images and similar to the methods proposed in [22] who reported an average lesion detection sensitivity rate of 90.98%. For the autonomous controller, the output of the image detection system is simply the pixel co-ordinates that correlate to the center-mass point of the detected target. This output offers a modular approach, with the ability to substitute the chosen detection approach with other modalities. For example, it could be replaced with the option of letting the user manually select a target themselves.

3) Stereo target position estimation: Here we use a stereo vision approach, with knowledge of the MFE camera pose at
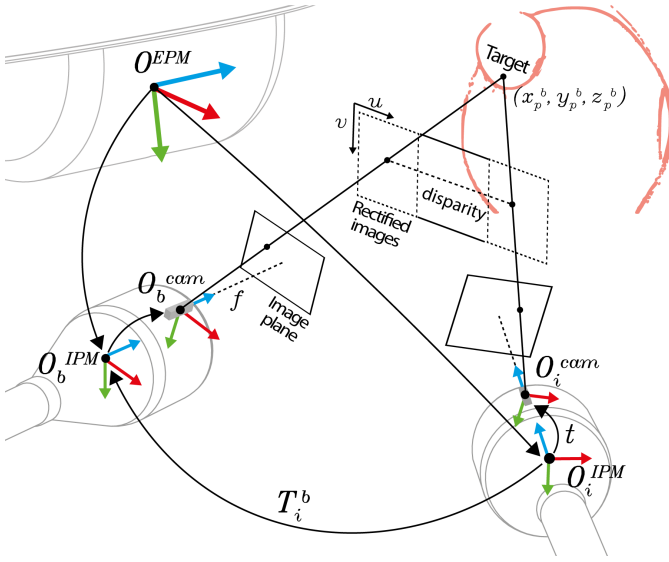
Fig. 3. Theoretical model of MFE stereo target position estimation approach.

two arbitrary positions, obtained from the magnetic localisation system, to compute distance to a tissue target (Fig. 3). This depth information is necessary to align the biopsy forceps, projected out from the tool channel at the same depth, to the target. First, the pixel co-ordinates of the target are identified in an initial base image plane, $m_b = (u_b, v_b)$, where (u_b, v_b) are the pixel coordinates of the target with O_b^{IPM} denoting the base pose of the IPM, with a known transformation, t, to the camera pose, O_b^{cam}. The MFE is then moved to an arbitrary, secondary pose where the location of the target is again identified $m_i = (u_i, v_i)$, in the inspection image plane and where O_i^{cam} denotes the secondary pose of the camera, w.r.t the base reference frame. The known rotation and transformation between the base camera pose and inspection camera pose, obtained from the magnetic localisation system, allows for the two images to be rectified to a common parallel plane.

With this, the disparity of the target between the two rectified images can be used to re-project the target to its real-world 3D coordinates using:

$$[X\,Y\,Z\,W] = H \times [u_b\,v_b\,disparity\,1]^T \tag{4}$$

$$z_p^b = Z/W \tag{5}$$

$$x_p^b = \frac{u_r - c_x}{f_x} \times z_p^b \tag{6}$$

$$y_p^b = \frac{v_r - c_y}{f_y} \times z_p^b \tag{7}$$

Where $[x_p^b, y_p^b, z_p^b]$ are the 3D co-ordinates of the target w.r.t. the base reference frame, H is the perspective transform matrix, (f_x, f_y) are the camera focal lengths, (c_x, c_y) is the camera principal point, and $disparity$ is the u pixel co-ordinate difference of the target between the two rectified images.

With these target co-ordinates saved, the euclidean distance between the target and any new pose of the MFE is then constantly updated using the magnetic localisation system, removing dependency on sufficient disparity in the stereo system. Firstly, the current position of the MFE camera (P_c) is remapped to be defined w.r.t the base camera reference frame:

$$\begin{bmatrix} x_c^b \\ y_c^b \\ z_c^b \end{bmatrix} = R_b^T P_c - R_b^T P_b \tag{8}$$

With the rotation matrix and position of the base camera w.r.t. the global reference frame defined as R_b and P_b, respectively. The distance between the current position of the MFE camera and the target is then constantly updated at every time-step using:

$$d = \sqrt{(x_c^b - x_p^b)^2 + (y_c^b - y_p^b)^2 + (z_c^b - z_p^b)^2} \tag{9}$$

This method assumes that the target remains static and that changes in depth are updated as consequence of motions of the MFE, and not of the target.

4) Instrument alignment: With the depth to the target obtained, the goal now is to impart a magnetic torque upon the IPM, such that the center of the tissue target in the camera image plane is aligned to a secondary pixel point, corresponding to the tip location of the biopsy forceps, when projected out from the tool channel at the same depth as the target.

Given the estimated depth from the target to the MFE camera defined in Eq. 9, the estimated pixel co-ordinates for the tip of the biopsy forceps are defined as:

$$\begin{bmatrix} u_t \\ v_t \end{bmatrix} = \begin{bmatrix} f\frac{t_x}{d_c^t} + \frac{w}{2} \\ f\frac{t_y}{d_c^t} + \frac{h}{2} \end{bmatrix} \tag{10}$$

with the pixel width and height of the image defined as w and h, respectively, f as the camera focal length, and t as the linear translation from the camera center to the tool channel center. A PI controller then aligns the centre of the target (u_p, v_p) with the tip of the estimated tool projection (u_t, v_t):

$$\begin{bmatrix} \delta\boldsymbol{\theta_x} \\ \delta\boldsymbol{\theta_y} \end{bmatrix} = \begin{bmatrix} (u_p - u_t) \\ (v_p - v_t) \end{bmatrix} \tag{11}$$

where $\delta\boldsymbol{\theta_y}$ and $\delta\boldsymbol{\theta_z}$ serves as the input to the endoscope orientation controller previously defined in Eq. 2. When the error between the tool tip projection and target has been minimised to below a defined tolerance, the user is prompted to perform a biopsy. Following this, the user may exert the forceps from the tool channel and obtain a sample of the tissue target. A full demonstration of this sequence is shown in Fig. 4, as well as Supplementary Video 1.

D. Random quadrant biopsy

This section describes the developed autonomous routine that attempts to sequentially align the MFE camera frame to 4 quadrants of the colon wall, equating to relative positions of the MFE camera frame at the 12, 3, 6, and 9 o'clock positions, shown in Fig. 10. In this mode, the $\delta\boldsymbol{\theta_y}$ and $\delta\boldsymbol{\theta_z}$ inputs of the orientation controller are computed by adding a fixed angle
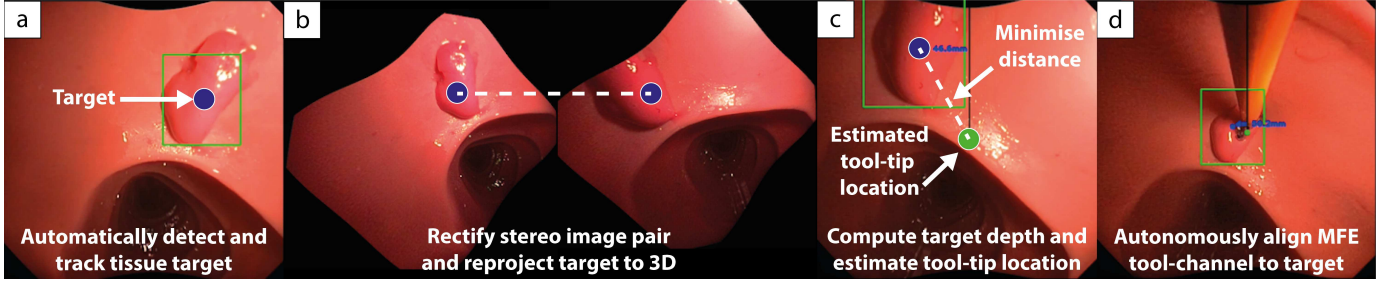
Fig. 4. Targeted biopsy sequence. **a**, The target is automatically detected and tracked. **b**, Two images of the target are acquired and rectified as a stereo pair. **c**, The depth to the target is computed and used to estimate the location of the tool-tip in the camera frame. **d**. Torque is imparted on the MFE to minimise the error between the target and tool-tip.

(25 degrees in this case) to the current orientation of the MFE camera frame. The sequence is controlled by switching the control variables $\alpha, \beta \in [-1, 0, 1]$ (12 o'clock: $\alpha = 1$, $\beta = 0$, 3 o'clock $\alpha = 0$, $\beta = 1$ etc...).

$$\begin{bmatrix} \delta\boldsymbol{\theta_x} \\ \delta\boldsymbol{\theta_y} \end{bmatrix} = \begin{bmatrix} \alpha & 0 \\ 0 & \beta \end{bmatrix} \begin{bmatrix} 25_{deg} \\ 25_{deg} \end{bmatrix} \tag{12}$$

Using a Graphical User Interface (GUI), the user can press a button to initiate the routine. Upon doing so, the autonomous routine will tilt the MFE camera to the heading of the first quadrant. Once the user has taken a biopsy at this location, they may press the button again to autonomously move to the next quadrant. This is repeated until all 4 quadrants have been visited.

When no input is given to the orientation controller, for example when all 4 quadrant biopsies have been taken, the system will enter the "magnet following" state (Section. II-C1) to keep the EPM and IPM in close proximity to each other. This allows the user to perform random quadrant biopsy at multiple locations, as the EPM will autonomously follow as the user withdraws the MFE by pulling back on the endoscope tether.

E. Closed-loop tele-operation

In this work, the performance of the high-level autonomous routines for random and targeted biopsy are compared against a lower-level, closed-loop tele-operated system; a known effective control approach for magnetic endoscopy validated in previous work from our group [7]. Here, using a 4-DOF joystick (Xbox adaptive controller, Microsoft), the user inputs how they wish to orientate the endoscope camera inside the colon. With this mode, the $\delta\boldsymbol{\theta_y}$ and $\delta\boldsymbol{\theta_z}$ inputs of the orientation controller described in Eq. 2 are simply defined as:

$$\begin{bmatrix} \delta\boldsymbol{\theta_x} \\ \delta\boldsymbol{\theta_y} \end{bmatrix} = \overline{\delta\theta_{a,I}} \tag{13}$$

with defined as user inputs from the joystick controller. Again, when no user input is given, the system will enter the "magnet following" state (Section. II-C1) to keep the EPM and IPM in close proximity to each other as the MFE is withdrawn.

III. EXPERIMENTAL VALIDATION

We first evaluated the accuracy of the MFE stereo positional reconstruction system to gauge its effectiveness at estimating the 3D location of a tissue target. Following this, we conducted a set of experiments on bench-top to evaluate the developed autonomous control strategies for targeted and random quadrant biopsy, with their respective performances being scored in terms of tissue acquisition time and user workload.

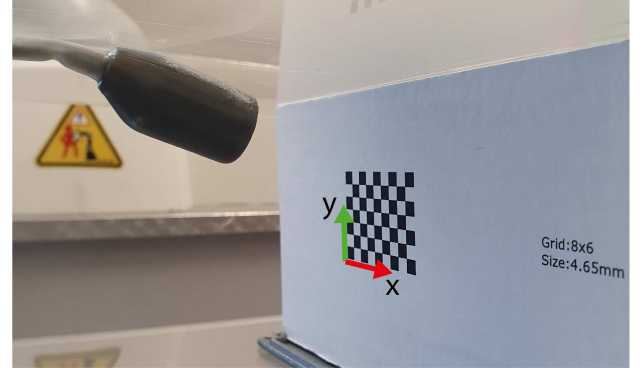### A. MFE Stereo reconstruction

Fig. 5. Experimental setup of checkerboard for validating MFE stereo target reconstruction system.

Method: A checkerboard (Grid: 8x6, Square size: 4.65mm) was mounted in a fixed location (Fig. 5). A transformation matrix T_W^C between the world reference frame (robot base) and the checkerboard reference frame (lower left grid corner) was defined using the known Cartesian pose of the robotic manipulator end effector, positioned and registered to the same pose as the checkerboard origin. The MFE stereo system was then used to reconstruct the 3D position of the checkerboard corners in 5 arbitrary camera configurations, with differing relative positions and roll, pitch, and yaw camera angles. A ground truth for the MFE camera trajectory and position of the checkerboard corner points was obtained using [23]. The resulting 3D reconstruction of the checkerboard corner points, and trajectory of the MFE camera from the localisation system (both defined with respect to the world reference frame) were defined with respect to the checkerboard ground truth origin, using the aforementioned transformation matrix

T_W^C. Positional errors between the checkerboard corner points ground truth, and stereo-reconstructed points were used to compare and quantify the accuracy of the MFE stereo system.

Results: Results of the MFE stereo target reconstruction are shown in Fig 6. The average absolute positional error of the reconstructed checkerboard corner points was 6.74mm $\pm$ 2.78mm.
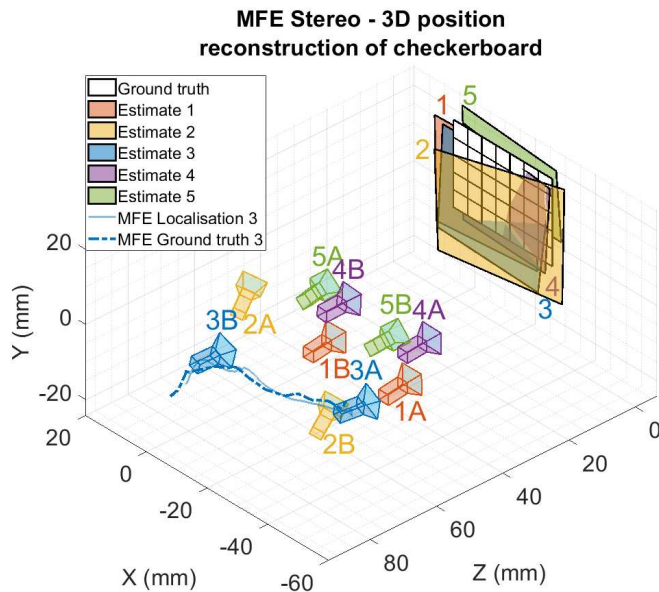

Fig. 6. MFE stereo system: 3D positional reconstruction of a checkerboard target. An initial camera pose 1-5A, and secondary camera pose 1-5B, combined with the MFE localisation system is used to reconstruct the 3D position of a checkerboard target (checkerboard reconstruction numbered 1-5). An example of the MFE camera trajectory obtained from the localisation system is shown with a corresponding ground truth for estimate 3.
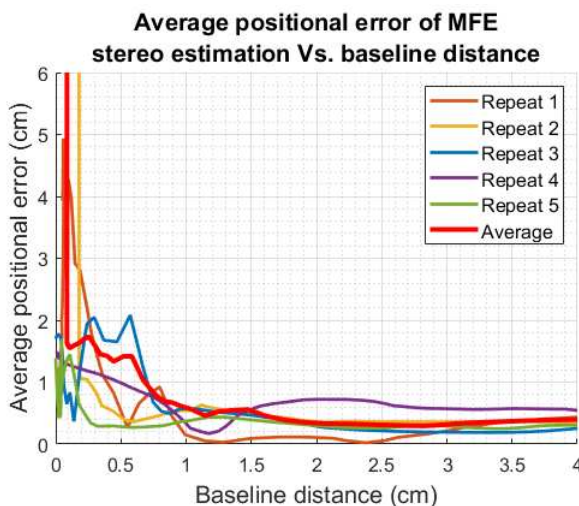

Fig. 7. Positional error of MFE stereo reconstruction system with varying baseline distance (camera distance between stereo image pair).

It was observed that the positional error of the target increased exponentially when the distance between the two camera pairs (baseline distance) was less than 1cm. This is shown in Fig. 7. With this, when the MFE camera first detects a tissue target, subsequent motions of the EPM during the autonomous biopsy routine will attempt to move the MFE to a secondary position, with depth only being computed when the MFE is at least 1cm away from the initial position where the target was first observed (base image). This is to ensure accurate depth estimation for the autonomous routine. This distance is reasonable considering the average diameter of the human colon is 4.7cm $\pm$ 0.5cm [24].

B. Targeted biopsy

Here we compare user performance for targeted biopsy using the following approaches: standard FE, MFE with closed-loop tele-operation, and MFE with semi-autonomous assistance.
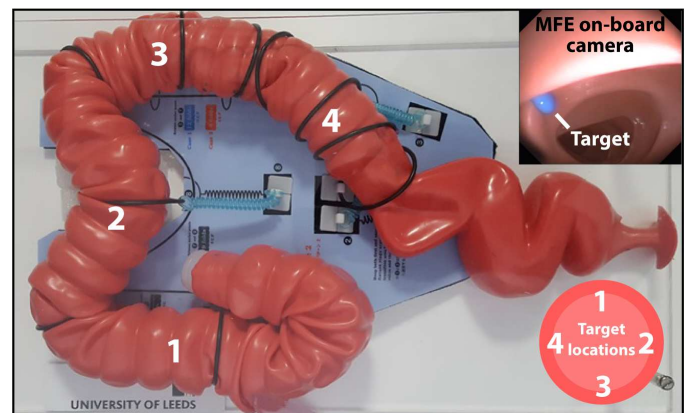

Fig. 8. Targeted biopsy experimental setup: Locations of biopsy targets (top right) inside latex colonoscopy training phantom (M40, Kyoto Kagaku Co.).

Method: In order to compare the effectiveness of each approach, 4 targets (3-4mm diameter, blue coloured polyvinyl acetate glue) were placed in a latex colonoscopy training phantom (M40, Kyoto Kagaku Co.), at various locations and quadrants. A bright target colour was chosen to be distinctively visible to the user to remove variations in time caused by an operator not being able to locate the target in non-autonomous repetitions. The locations are shown in Fig. 8, with target 1 placed in the ascending colon at the 12 o'clock position, target 2 was placed in the transverse at the 3 o'clock position, target 3 was placed in the descending colon at the 6 o'clock position, and finally target 4 was placed in the sigmoid colon at the 9 o'clock position.

For each approach, the scope was placed at the cecum and operators were instructed to pull back on the scope to withdraw from the colon. When the user visualised and identified the first target, they were given a 10 minute time limit [25] to perform a biopsy of that target. Upon successfully taking a biopsy, confirmed by withdrawing the forceps from the tool channel and noting a satisfactory sample with a weight $\geq$ 0.01g, or failing by exceeding the 10 minute time limit without a valid sample, operators were instructed to continue withdrawing until reaching the next target. This was repeated until fully withdrawn and with all targets visited, with the time to perform a biopsy at each site, and success rate at each site recorded. Upon completing the task, operators completed a NASA task load index form, a widely used workload

This article has been accepted for publication in IEEE Transactions on Medical Robotics and Bionics. This is the author's version which has not been fully edited and content may change prior to final publication. Citation information: DOI 10.1109/TMRB.2022.3187028

7

assessment tool that aims to score human perceived workload on six subjective sub-scales [26].

The experimental scheme was completed by 3 operators with no prior endoscopic experience, with an assistant present to pass the biopsy forceps down the tool channel and take a biopsy as this action could disturb the orientation of the endoscope, requiring the operator to remain in control. With each user, repetitions were randomised to use either the standard FE, MFE with closed-loop control, or MFE with autonomous control until 5 repetitions had been performed for each of the 3 methods (15 total for each user).

Results: Times for targeted biopsy, from first visualising a tissue target, to successfully removing a valid sample are shown below in Fig, 9. The mean average time for the standard FE was 1min 54s $\pm$ 1min 44s. The MFE with closed-loop tele-operation presented the fastest time on average with a time of 1min 30s $\pm$ 1min 09s. The MFE semi-autonomous routine had a respectable average time of 2min 23s $\pm$ 1min 43s. Success rates for the standard FE, MFE with closed-loop tele-operation, and MFE semi-autonomous operation were 100%, 100% and 95%, respectively. In-complete attempts using the semi-autonomous approach were due to the haustral folds present in the colon. In certain positions, these anatomical features would randomly block the view of the target during alignment, or cause the target to be in-properly illuminated. This would cause the autonomous routine to lose tracking, and not be able to align the target during the time-limit. This could be rectified by sufficiently insufflating and distending the colon to reduce the prominence and blocking effect of the folds.
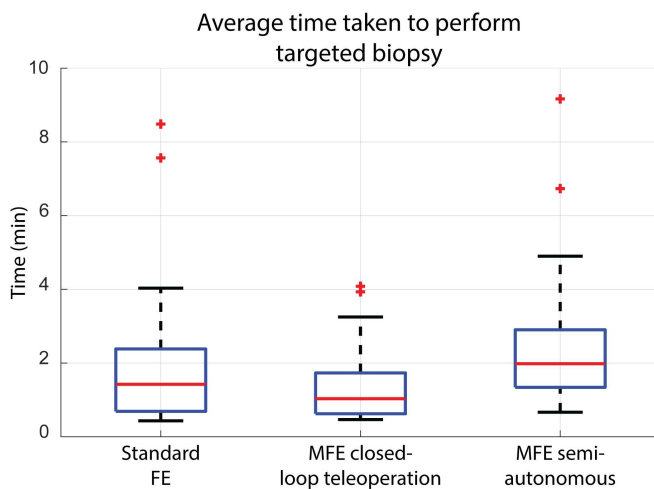
Average time taken to perform targeted biopsy

Fig. 9. Targeted biopsy times: Standard FE, n=60; MFE closed-loop tele-operation, n=60; MFE semi-autonomous, n=57. Red bars indicate median, edges are 25th and 75th percentiles, whiskers indicate range, red crosses denote outliers.

In terms of user workload, shown in Table. I, operators found the standard FE to be more physically and mentally demanding, having to physically overcome resistance in the scope control interface to maintain orientation on the target, while giving inputs that seemingly resulted in a random motion of the scope camera. This also resulted in higher levels of effort and frustration. In comparison, both approaches with

TABLE I
NASA TASK LOAD INDEX MEAN OPERATOR WORKLOAD RATINGS FOR TARGETED BIOPSY RESULTS

Subscale	Targeted biopsy: Unweighted mean workload ratings (lower score better)		
	Standard FE	MFE closed-loop teleop	MFE semi-autonomous
Mental demand	59.5	18.8	10.5
Physical demand	79.0	13.8	12.5
Temporal demand	37.5	21.3	23.5
Performance	33.0	31.3	29.5
Effort	69.0	26.3	21.0
Frustration	64.0	40.0	22.0

the MFE reduced workload in all categories, with the semi-autonomous routine presenting significantly lower scores for mental demand, effort and frustration, as most responsibility was given to the autonomous system, letting the operator take on a more super-visionary role.

C. Random quadrant biopsy

Here we compare user performance for random quadrant biopsy when using a standard FE, using the MFE with closed-loop tele-operation, and using the MFE with semi-autonomous assistance.

Method: The experimental setup is shown in Fig. 10. An acrylic tube was used to arrange a phantom tissue substrate in to a hollow cylinder, with a length of 450mm, diameter of 45mm, and thickness $\approx$ 5mm, and was made from cast silicone (Ecoflex 00-10 silicone). This setup was chosen as it suitably allowed for a repeatable, destructive model removing material with a large number of biopsy attempts.
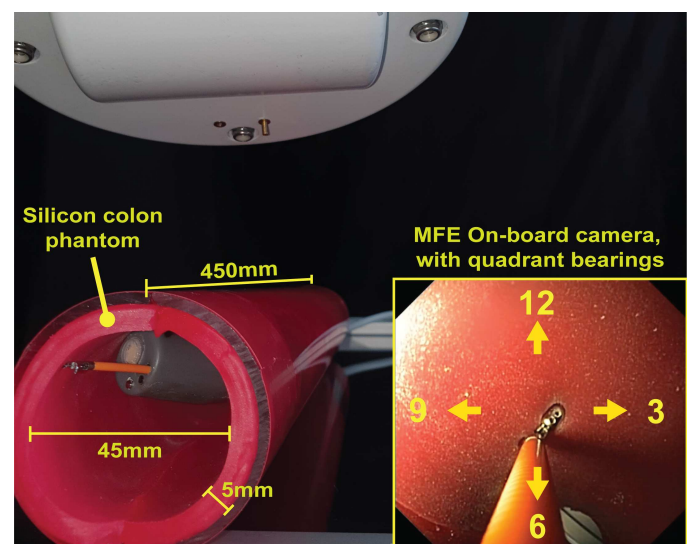
Fig. 10. Random quadrant biopsy experimental setup. A silicone (Ecoflex 00-10) colon phantom (450mm length, 45mm diameter, 5mm thickness) was used to perform 4 random quadrant biopsies at 3, 10cm intervals. An on-board view of the MFE camera is shown (bottom right).

During each repetition, the endoscope was placed at the distal end of the tube and withdrawn by hand. At each 10cm interval, measured by markings on the endoscope shaft, the

This article has been accepted for publication in IEEE Transactions on Medical Robotics and Bionics. This is the author's version which has not been fully edited and content may change prior to final publication. Citation information: DOI 10.1109/TMRB.2022.3187028

8

operator was instructed to perform 4 biopsies from each quadrant (3, 6, 9, and 12 o'clock position) before continuing to withdraw. This was repeated 3 times at every 10cm interval for a total of 12 biopsies. Evaluation of a successful sample was performed for each bite by confirming a sample weight $\geq$ 0.005g, being a similarly dimensioned sample, but a slightly less dense material than used in the targeted experimental setup. Repetitions were randomised to use either the standard FE, MFE with closed-loop tele-operation, or MFE with autonomous control until 5 repetitions had been performed for each of the 3 methods (15 attempts for each operator). The experimental scheme was completed by 3 operators with no prior endoscopic experience, with an assistant present to pass the biopsy forceps down the tool channel and take a biopsy. After each repetition, users were asked to complete a NASA task load assessment form to compare the ease of use of the different approaches.

Results: An example trajectory for the MFE performing semi-autonomous, random quadrant biopsy is shown in Fig. 11, and was obtained from the magnetic localisation system. The orientation of the MFE (red arrows) can be seen directed to 4 quadrants of the colon at 3 locations, with each location being separated by $\approx$10cm.
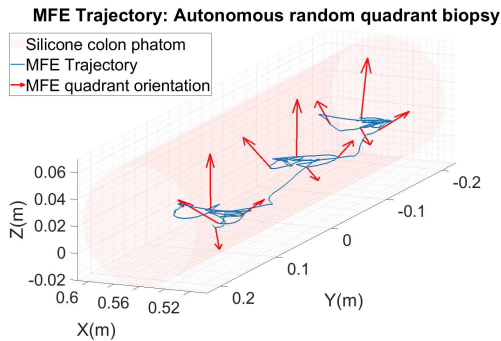

Fig. 11. MFE trajectory when performing semi-autonomous, random quadrant biopsy in a silicone phantom colon.

Times to complete 4 biopsies from each quadrant are shown in Fig. 12, for each of the different approaches. The mean average times for the standard FE and MFE with closed-loop tele-operation were similar with times of 2min 12s $\pm$ 17s and 2min 32s $\pm$ 18s, respectively. The MFE semi-autonomous presented a mean average time of 3min 11s $\pm$ 23s. All of the 3 approaches were 100% successful at obtaining a valid tissue sample during each biopsy attempt. Regarding user workload, results are shown in Table. II.

Users found the standard FE to be more physically demanding and require more effort when compared to both approaches using the MFE. The MFE semi-autonomous routine produced significantly lower scores for mental demand and effort, as most of the workload is offloaded to the autonomous system, simplifying the involvement of the operator.

IV. DISCUSSION

In this paper, we have developed and investigate the role of autonomy for performing targeted and random quadrant biopsy with an intelligent magnetic endoscope. As magnetic
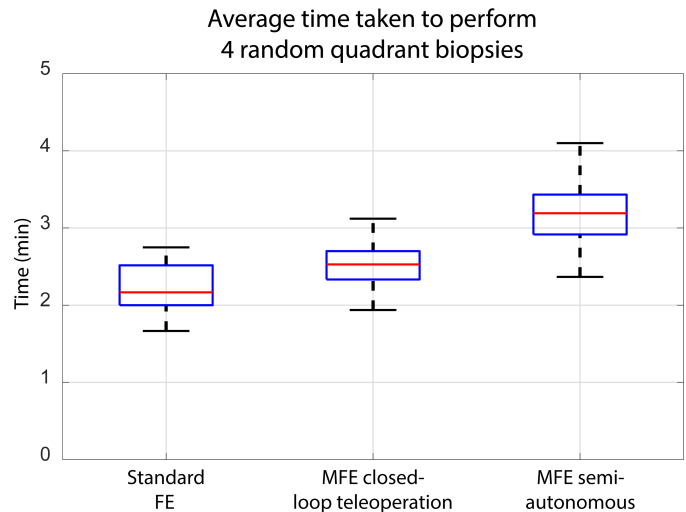

Fig. 12. Average time to perform 4 random quadrant biopsies: Standard FE, n=45; MFE closed-loop tele-operation, n=45; MFE semi-autonomous navigation, n=45. Red bars indicate median, edges are 25th and 75th percentiles, whiskers indicate range.

TABLE II
NASA TASK LOAD INDEX MEAN OPERATOR WORKLOAD RATINGS FOR
RANDOM QUADRANT BIOPSY RESULTS

Subscale	Random quadrant biopsy: Unweighted mean workload ratings (lower score better)		
	Standard FE	MFE closed-loop teleop	MFE semi-autonomous
Mental demand	23.5	23.0	15.0
Physical demand	73.5	15.0	11.5
Temporal demand	27.0	30.0	27.0
Performance	27.0	30.0	23.5
Effort	47.0	24.5	17.0
Frustration	27.5	23.5	20.5

endoscopes transition in to clinical use for procedures such as colonoscopy, an ability to effectively perform all procedural aspects should be present. However, the focus of investigation for improving clinical performance and ease-of-use has mainly been concerned with general endoscope navigation through robotic-assisted autonomy. Numerous works for mechanically actuated endoscopes have commented on autonomy reducing cost and user learning-curve whilst increasing endoscopic efficiency with im-proved access to providers [27], [28], [29], [17]. This is encouraging and justifies developments in autonomy for other actuation approaches such as magnetic endoscopy where remarks of ease-of-use are comparatively more sparse [7], [5]. Therefore, our focus in this work is concerned with the role of autonomy for targeted and random quadrant biopsy in the colon, but being applicable to multiple scenarios in the body where control over magnetic endoscopes is required in complex environments.

We show that the developed semi-autonomous routines reduce the cognitive workload placed on the operator, requiring less effort to perform a targeted or random quadrant biopsy task. Furthermore, we show that the semi-autonomous routines are able to achieve comparable times to a standard FE, while requiring minimal involvement from the operator. We show

that the semi-autonomous targeted routine was able to orientate the magnetic endoscope with high precision, achieving effective alignment to a small target with a diameter of 3-4mm. In the future, the robot speed will be increased to achieve faster motion and further reduce duration. Combined with the demonstrated reduced user workload, this has potential benefits in reducing training costs and time, allowing previously required training resources to be better utilised and letting operators focus even more on the diagnosis and treatment of patients.

The adopted stereo system for acquiring positional information of a tissue target is sufficient for demonstrating the capabilities of a semi-autonomous targeted biopsy system, but a more advanced method should be further investigated for use in an in-vivo setting. This is due to the stereo-concept assuming that the target remains stationary, and that points can be effectively matched between the two images which may present inaccuracies in the presence of peristalsis and patient movement, in-vivo. With the modular nature of the developed semi-autonomous routines, a more advance vision system can be easily adopted.

The developed semi-autonomous biopsy routines present the option for a single operator approach. Conventionally, the operator is needed to maintain control over the endoscope orientation to counteract disturbances, while an assistant inserts, grasps, and withdraws the biopsy forceps. In situations without an assistant, the operator would first need to manually establish a stable position before freeing a hand from the controls to operate the biopsy forceps. With the autonomous system, stability was immediately and constantly maintained by the controller and would allow a single user to perform the function of acquiring a tissue sample. This is particularly pertinent given the current COVID-19 pandemic. During colonoscopy, conventional approaches using a standard FE require multiple staff and the patient to be within close proximity. This is problematic, as FEs generate aerosols that can readily spread infection between the multiple, grouped personnel [30]. With this, further work should investigate magnetic endoscope stability control in-vivo, with the presence of additional disturbances such as patient breathing and peristalsis to further demonstrate capabilities of maintaining stability, and a single user approach.

REFERENCES

[1] D. A. Joseph, R. G. Meester, A. G. Zauber, D. L. Manninen, L. Winges, F. B. Dong, B. Peaker, and M. van Ballegooijen, "Colorectal cancer screening: estimated future colonoscopy need and current volume and capacity," *Cancer*, vol. 122, no. 16, pp. 2479–2486, 2016.

[2] F. Bray, J. Ferlay, I. Soerjomataram, R. L. Siegel, L. A. Torre, and A. Jemal, "Global cancer statistics 2018: Globocan estimates of incidence and mortality worldwide for 36 cancers in 185 countries," *CA: a cancer journal for clinicians*, vol. 68, no. 6, pp. 394–424, 2018.

[3] I. Kassim, L. Phee, W. S. Ng, F. Gong, P. Dario, and C. A. Mosse, "Locomotion techniques for robotic colonoscopy," *IEEE Engineering in Medicine and Biology Magazine*, vol. 25, no. 3, pp. 49–56, 2006.

[4] S. Larsen, A. Kalloo, and S. Hutfless, "The hidden cost of colonoscopy including cost of reprocessing and infection rate: the implications for disposable colonoscopes," *Gut*, vol. 69, no. 2, pp. 197–200, 2020.

[5] A. P. Mamunes, F. Campisano, J. Martin, B. Scaglioni, E. Mazomenos, P. Valdastri, and K. L. Obstein, "Magnetic flexible endoscope for colonoscopy: an initial learning curve analysis," *Endoscopy International Open*, vol. 9, no. 02, pp. E171–E180, 2021.

[6] J. C. Norton, P. R. Slawinski, H. S. Lay, J. W. Martin, B. F. Cox, G. Cummins, M. P. Desmulliez, R. E. Clutton, K. L. Obstein, S. Cochran, and P. Valdastri, "Intelligent magnetic manipulation for gastrointestinal ultrasound," *Science Robotics*, vol. 4, no. 31, jun 2019. [Online]. Available: http://robotics.sciencemag.org/

[7] J. W. Martin, B. Scaglioni, J. C. Norton, V. Subramanian, A. Arezzo, K. L. Obstein, and P. Valdastri, "Enabling the future of colonoscopy with intelligent and autonomous magnetic manipulation," *Nature Machine Intelligence*, vol. 2, no. 10, pp. 595–606, oct 2020. [Online]. Available: https://doi.org/10.1038/s42256-020-00231-9

[8] N. Shamsudhin, V. I. Zverev, H. Keller, S. Pane, P. W. Egolf, B. J. Nelson, and A. M. Tishin, "Magnetically guided capsule endoscopy," *Medical physics*, vol. 44, no. 8, pp. e91–e111, 2017.

[9] M. Verra, A. Firrincieli, M. Chiurazzi, A. Mariani, G. Lo Secco, E. Forcignanò, A. Koulaouzidis, A. Menciassi, P. Dario, G. Ciuti, and A. Arezzo, "Robotic-Assisted Colonoscopy Platform with a Magnetically-Actuated Soft-Tethered Capsule," *Cancers*, vol. 12, no. 9, p. 2485, sep 2020. [Online]. Available: https://www.mdpi.com/2072-6694/12/9/2485

[10] S.-Y. Yen, H.-E. Huang, G.-S. Lien, C.-W. Liu, C.-F. Chu, W.-M. Huang, and F.-M. Suk, "Automatic lumen detection and magnetic alignment control for magnetic-assisted capsule colonoscope system optimization," *Scientific reports*, vol. 11, no. 1, pp. 1–10, 2021.

[11] K. M. Popek, T. Hermans, and J. J. Abbott, "First demonstration of simultaneous localization and propulsion of a magnetic capsule in a lumen using a single rotating magnet," in *Proceedings - IEEE International Conference on Robotics and Automation*. IEEE, may 2017, pp. 1154–1160. [Online]. Available: http://ieeexplore.ieee.org/document/7989138/

[12] P. R. Slawinski, A. Z. Taddese, K. B. Musto, K. L. Obstein, and P. Valdastri, "Autonomous Retroflexion of a Magnetic Flexible Endoscope," *IEEE Robotics and Automation Letters*, vol. 2, no. 3, pp. 1352–1359, 2017. [Online]. Available: http://ieeexplore.ieee.org/document/7852481/

[13] M. Verra, A. Firrincieli, M. Chiurazzi, A. Mariani, G. Lo Secco, E. Forcignanò, A. Koulaouzidis, A. Menciassi, P. Dario, G. Ciuti *et al.*, "Robotic-assisted colonoscopy platform with a magnetically-actuated soft-tethered capsule," *Cancers*, vol. 12, no. 9, p. 2485, 2020.

[14] Y. Li, C. Guo, W. Xin, T. Pan, W. Li, P. W. Y. Chiu, and Z. Li, "Design and Preliminary Evaluation of an Electromagnetically Actuated Soft-Tethered Colonoscope," *IEEE Transactions on Medical Robotics and Bionics*, vol. 3, no. 2, pp. 402–413, mar 2021.

[15] P. Valdastri, G. Ciuti, A. Verbeni, A. Menciassi, P. Dario, A. Arezzo, and M. Morino, "Magnetic air capsule robotic system: Proof of concept of a novel approach for painless colonoscopy," *Surgical Endoscopy and Other Interventional Techniques*, vol. 26, no. 5, pp. 1238–1246, 2012.

[16] M. Simi, G. Gerboni, A. Menciassi, and P. Valdastri, "Magnetic torsion spring mechanism for a wireless biopsy capsule," *Journal of Medical Devices*, vol. 7, no. 4, 2013.

[17] Q. Zhang, J. M. Prendergast, G. A. Formosa, M. J. Fulton, and M. E. Rentschler, "Enabling Autonomous Colonoscopy Intervention Using a Robotic Endoscope Platform," *IEEE Transactions on Biomedical Engineering*, vol. 68, no. 6, pp. 1957–1968, jun 2021. [Online]. Available: https://pubmed.ncbi.nlm.nih.gov/33296299/

[18] A. Peixoto, M. Silva, P. Pereira, and G. Macedo, "Biopsies in gastrointestinal endoscopy: when and how," *GE Portuguese journal of gastroenterology*, vol. 23, no. 1, pp. 19–27, 2016.

[19] A. Z. Taddese, P. R. Slawinski, M. Pirotta, E. De Momi, K. L. Obstein, and P. Valdastri, "Enhanced Real-Time Pose Estimation for Closed-Loop Robotic Manipulation of Magnetically Actuated Capsule Endoscopes Journal Title XX(X):1-25." [Online]. Available: www.sagepub.com/

[20] A. W. Mahoney and J. J. Abbott, "Five-degree-of-freedom manipulation of an untethered magnetic device in fluid using a single permanent magnet with application in stomach capsule endoscopy," *The International Journal of Robotics Research*, vol. 35, no. 1-3, pp. 129–147, 2016.

[21] J. Redmon and A. Farhadi, "YOLOv3: An Incremental Improvement," apr 2018. [Online]. Available: http://arxiv.org/abs/1804.02767

[22] J. Y. Lee, J. Jeong, E. M. Song, C. Ha, H. J. Lee, J. E. Koo, D. H. Yang, N. Kim, and J. S. Byeon, "Real-time detection of colon polyps during colonoscopy using deep learning: systematic validation with four independent datasets," *Scientific Reports*, vol. 10, no. 1, pp. 1–9, dec 2020. [Online]. Available: https://doi.org/10.1038/s41598-020-65387-1

[23] Z. Zhang, "A flexible new technique for camera calibration," *IEEE Transactions on Pattern Analysis and Machine Intelligence*, vol. 22, no. 11, pp. 1330–1334, nov 2000.

[24] A. Alazmani, A. Hood, D. Jayne, A. Neville, and P. Culmer, "Quantitative assessment of colorectal morphology: Implications for robotic colonoscopy," *Medical engineering & physics*, vol. 38, no. 2, pp. 148–154, 2016.

[25] E. M. Ritter, T. C. Cox, K. D. Trinca, and J. P. Pearl, "Simulated Colonoscopy Objective Performance Evaluation (SCOPE): A non-computer-based tool for assessment of endoscopic skills," *Surgical Endoscopy*, vol. 27, no. 11, pp. 4073–4080, jul 2013. [Online]. Available: https://link.springer.com/article/10.1007/s00464-013-3063-8

[26] S. G. Hart and L. E. Staveland, "Development of nasa-tlx (task load index): Results of empirical and theoretical research," in *Advances in psychology*.   Elsevier, 1988, vol. 52, pp. 139–183.

[27] B. Vucelic, D. Rex, R. Pulanic, J. Pfefer, I. Hrstic, B. Levin, Z. Halpern, and N. Arber, "The aer-o-scope: proof of concept of a pneumatic, skill-independent, self-propelling, self-navigating colonoscope," *Gastroenterology*, vol. 130, no. 3, pp. 672–677, 2006.

[28] E. Tumino, R. Sacco, M. Bertini, M. Bertoni, G. Parisi, and A. Capria, "Endotics system vs colonoscopy for the detection of polyps," *World Journal of Gastroenterology: WJG*, vol. 16, no. 43, p. 5452, 2010.

[29] N. Van der Stap, R. Reilink, S. Misra, I. A. M. J. Broeders, and F. van der Heijden, "The use of the focus of expansion for automated steering of flexible endoscopes," in *2012 4th IEEE RAS & EMBS International Conference on Biomedical Robotics and Biomechatronics (BioRob)*.   IEEE, 2012, pp. 13–18.

[30] O. Onaizah, Z. Koszowska, C. Winters, V. Subramanian, D. Jayne, A. Arezzo, K. L. Obstein, and P. Valdastri, "Guidelines for robotic flexible endoscopy at the time of covid-19," *Frontiers in Robotics and AI*, vol. 8, p. 20, 2021.